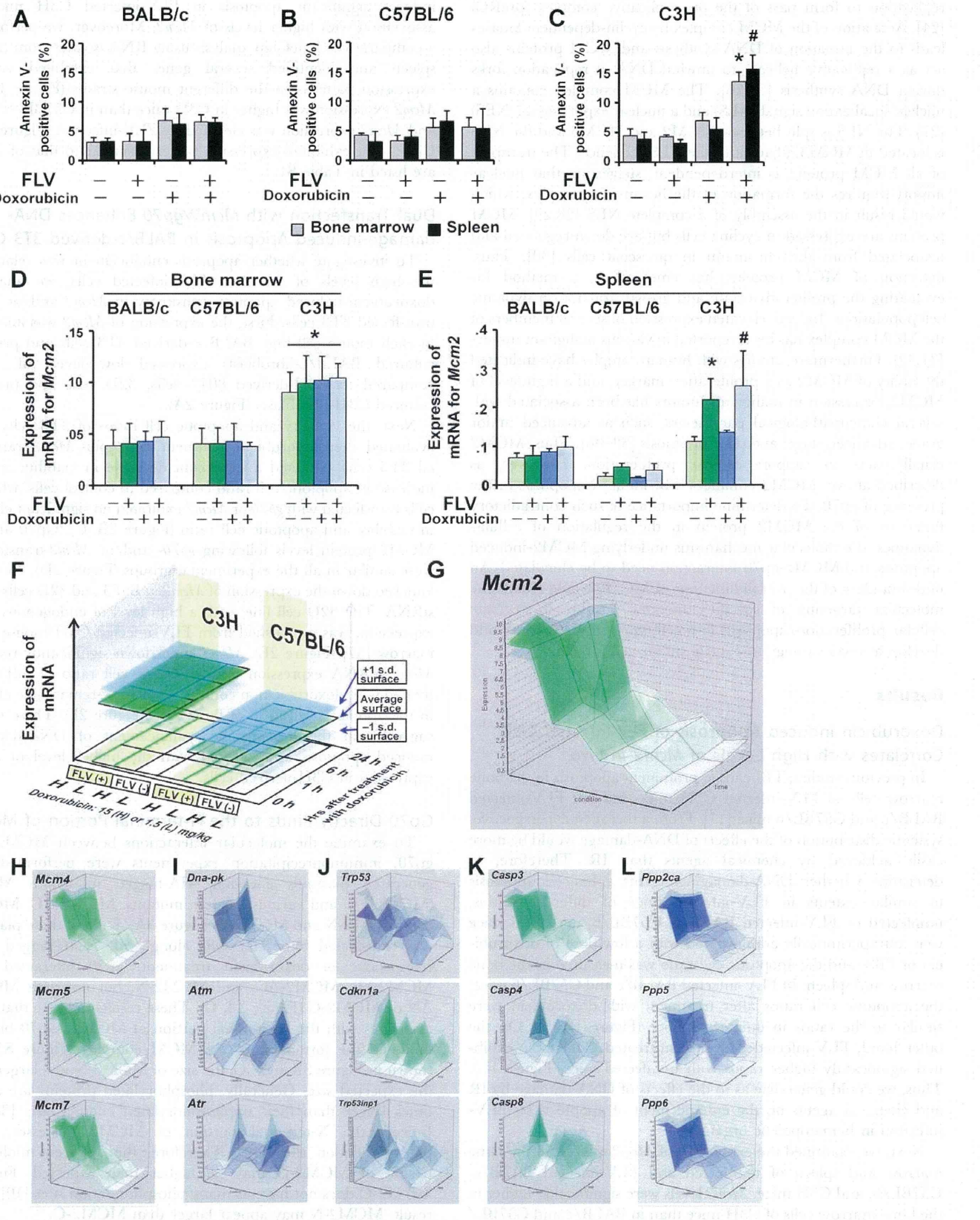

Figure 1. ***In vivo*** **assessment of doxorubicin-induced apoptosis and the associated changes in mRNA expression in FLV-infected mice.** Uninfected or FLV-infected BALB/c (A), C57BL/6 (B), and C3H (C) mice were intraperitoneally (i.p.) administrated with 1.5 mg/kg of doxorubicin or PBS, and the apoptotic cell ratios in the bone marrow (gray bars) and spleen cells (black bars) were determined 24 h later with annexin V-staining. Note the significant increase in the proportion of annexin V-positive cells in the bone marrow and spleen of FLV-infected C3H mice after the doxorubicin treatment compared to that in the bone marrow and spleen cells of uninfected mice "FLV (−), Doxorubicin (−)" (*$p<0.01$ and $^{\#}p<0.01$).

Data represent the mean and 95% confidence intervals (CI) of 3 independent experiments. (D) Quantitative RT-PCR analysis of *Mcm2* mRNA expression in the bone marrow of uninfected and FLV-infected BALB/c, C57BL/6, and C3H mice. The bone marrow cells of the C3H strain exhibit higher levels of *Mcm2* in all groups compared to the corresponding groups of BALB/c and C57BL/6 mice (*$p<0.01$, for each group). (E) Quantitative RT-PCR analysis of *Mcm2* mRNA expression in the spleen of uninfected and FLV-infected BALB/c, C57BL/6, and C3H mice. Spleen *Mcm2* expression is higher in the "FLV (+), Doxorubicin (−)" and "FLV (+), Doxorubicin (+)" C3H mice than in the corresponding groups of BALB/c and C57BL/6 mice (*$p<0.01$ and $^{\#}p<0.01$, respectively). In C3H mice, FLV-infection induces higher levels of *Mcm2* expression compared to the expression in uninfected mice. Data represent the mean and 95% CI from 5 mice in each group and are representative of 2 independent experiments. The GeneChip data for *Mcm*-associated and apoptosis-associated genes were analyzed using the Percellome method. Forty-eight male C57BL/6 and C3H mice were divided into 16 groups of 3 mice each. Uninfected or FLV-infected C57BL/6 and C3H mice were administered (i.p.) with 15 mg/kg (high dose) or 1.5 mg/kg (low dose) of doxorubicin, and the spleen was sampled 0, 1, 6, and 24 h after administration. The spleen transcriptome was measured using the Affymetrix Mouse 430-2 GeneChip. (F) The Percellome data were plotted on 3-dimensional graphs for average, +1 SD, and −1 SD surfaces as demonstrated in the left schema. The scale of expression (vertical axis) is the copy number per cell. The x-axis of the 3-dimensional graph shows the experimental groups, including the C3H and C57BL/6 mice with doxorubicin treatment (high and low doses) with or without FLV-infection. The y-axis shows the time course (0, 1, 6, and 24 h) after treatment with doxorubicin and the z-axis (vertical) indicates the intensity of mRNA expression of each gene. The data of each point are connected to form a surface illustration. The expression patterns of genes are compared using the surface images. (G) The *Mcm2* expression pattern is shown in the upper right box. Of the lower columns, the first column (H) shows the data for the genes of representative *Mcm* family members, the second column (I), PI3K members, the third column (J), p53-associated genes, the fourth column (K), caspase members and fifth column (L), protein phosphatase members (PPs). *Mcm* family members, *Dna-pk*, *caspase-3* (*Casp3*), *Ppp2ac*, and *Ppp6* exhibit gene expression patterns similar to that of *Mcm2*.

doi:10.1371/journal.pone.0040129.g001

The C-terminal Portion of MCM2 is Essential for the Enhancement of Doxorubicin-induced Apoptosis

Next, to identify the functional domain of MCM2 essential for apoptosis enhancement following DNA-damage, a functional analysis was performed using MCM2 deletion mutants. First, *Mcm2-FL* or the deletion mutant were introduced into 3T3 cells with or without *gp70*. After the transfection, 3T3 cells were treated with doxorubicin, and cell viability and apoptotic cell ratio were measured. 3T3 cells, transfected with *gp70* and the *Mcm2-FL* exhibited a significant decrease in viability and an increase in apoptotic cell ratio compared to cells transfected with the negative control (Figure 4A, B). Surprisingly, cells transfected with *gp70* and *Mcm2-ΔN-* or *Mcm2-C*, which did not interact with gp70, also exhibited a significant decrease in viability and an increase in apoptotic cell ratio relative to the negative control (Figure 4A, B). Among the cells singly transfected with *Mcm2-FL* or the mutants, *Mcm2-FL-*, *Mcm2-ΔC-*, and *Mcm2-N*-transfected cells exhibited no remarkable change in viability and apoptotic cell ratio compared to the negative control (Figure 4C, D). By contrast, *Mcm2-ΔN* and *Mcm2-C*-transfected cells exhibited a significant decrease in viability and an increase in apoptotic cell ratio (Figure 4C, D).

Previous studies have shown that MCM2 is essential for DNA replication [23,25], and its expression is up-regulated in proliferating cells [41]. *Mcm2*-transfected 3T3 cells exhibited no significant change in cell count during the early stage (Figure S3A, B). However, at a later-stage (96 h), the cell count was significantly higher in *Mcm2*-transfected 3T3 cells than in the control (Figure S3C, D).

We next examined the protein levels of DNA-PK, phospho-DNA-PK (pS2053), P53, phospho-P53, and cleaved caspase-3 in *Mcm2-FL-* or Mcm2 deletion mutant-transfected 3T3 cells after doxorubicin treatment. Among the cells transfected with *gp70* plus *Mcm2-FL-* or *gp70* plus mutant-transfected cells, *Mcm2-FL-*, *Mcm2-ΔN-*, and *Mcm2-C*-transfected cells expressed higher endogenous levels of DNA-PK, phospho-DNA-PK, P53, phospho-P53, and cleaved caspase-3 than the negative control (Figure 4E). By contrast, the levels of these proteins in *Mcm2-ΔC-* and *Mcm2-N*-transfected cells did not change (Figure 4E). Among the cells singly transfected with *Mcm2-FL* or a mutant, *Mcm2-ΔN-*, and *Mcm2-C*-transfected cells exhibited higher levels of DNA-PK, phospho-DNA-PK, P53, phospho-P53, and cleaved caspase-3 after doxorubicin treatment (Figure 4F). These results indicate that not only the binding of MCM2 with gp70 but also deletion of the N-terminal portion enhances DNA-damage-induced apoptosis via the activation of P53 by DNA-PK. Furthermore, MCM2 lacking the C-terminal portion did not induce apoptosis even with *gp70* co-expression indicating that the C-terminal portion of MCM2 was essential for the enhancement of DNA-damage-induced apoptosis.

DNA-PK is robustly activated by auto-phosphorylation at Ser 2056 (S2053 in mouse) in apoptotic cells [42], while phosphorylation at Thr 2609 is associated with non-homologous end joining [43]. Therefore, to examine whether DNA-PK was exclusively required for the enhancement of apoptosis, we inhibited DNA-PK activity using NU7026 in the presence (Figure 4G) or absence of *gp70* (Figure 4H). Inhibition of DNA-PK activity by NU7026 substantially reduced the level of phospho-DNA-PK (pS2053) and completely abolished apoptosis enhancement in cells expressing the *Mcm2 mutants* (Figure 4G, H). These results and knockdown experiments (Figure S4) indicate that DNA-PK activation is necessary for the enhancement of doxorubicin-induced apoptosis.

The Gp70-MCM2 Complex Binds to PP2A and Causes Hyperphosphorylation of DNA-PK

To determine the mechanism by which the gp70-MCM2 complex activated DNA-PK to enhance apoptosis, we sought to identify the upstream regulatory factors of DNA-PK. We focused on protein phosphatase 2A (PP2A), because this molecule has been shown to dephosphorylate DNA-PK and control its function [44–46]. 3T3 cells were transfected with *Mcm2-FL* or *Mcm2* deletion mutants with or without *gp70* and treated with doxorubicin. In the absence of *gp70*, PP2A did not interact with MCM2-FL or the mutants (Figure 5A, left). In *gp70*-transfected cells, PP2A co-precipitated with MCM2-FL, MCM2-ΔN, and MCM2-C, but not with MCM2-ΔC or MCM2-N (Figure 5A, right). Thus, PP2A interact with the C-terminal portion of MCM2 in *gp70*-transfected 3T3 cells.

To determine whether the enhanced apoptosis was caused by the inactivation of PP2A, the PP2A-specific inhibitor okadaic acid (OA) was added to 3T3 cells that were treated with doxorubicin. As expected, the OA-treated 3T3 cells exhibited a significant increase in apoptotic cell ratio compared to the control (Figure 5B). Furthermore, NU7026 treatment abrogated the doxorubicin-induced apoptosis enhancement in OA-treated 3T3 cells (Figure 5B). The expression of phospho-DNA-PK (pS2053) was upregulated in OA-treated 3T3 cells after doxorubicin treatment (Figure 5C). These results suggest that the gp70-MCM2 complex binds to and inhibits PP2A. Consequently, DNA-PK is hyperphosphorylated and doxorubicin-induced apoptosis is enhanced via the P53/cleaved caspase-3 pathway.

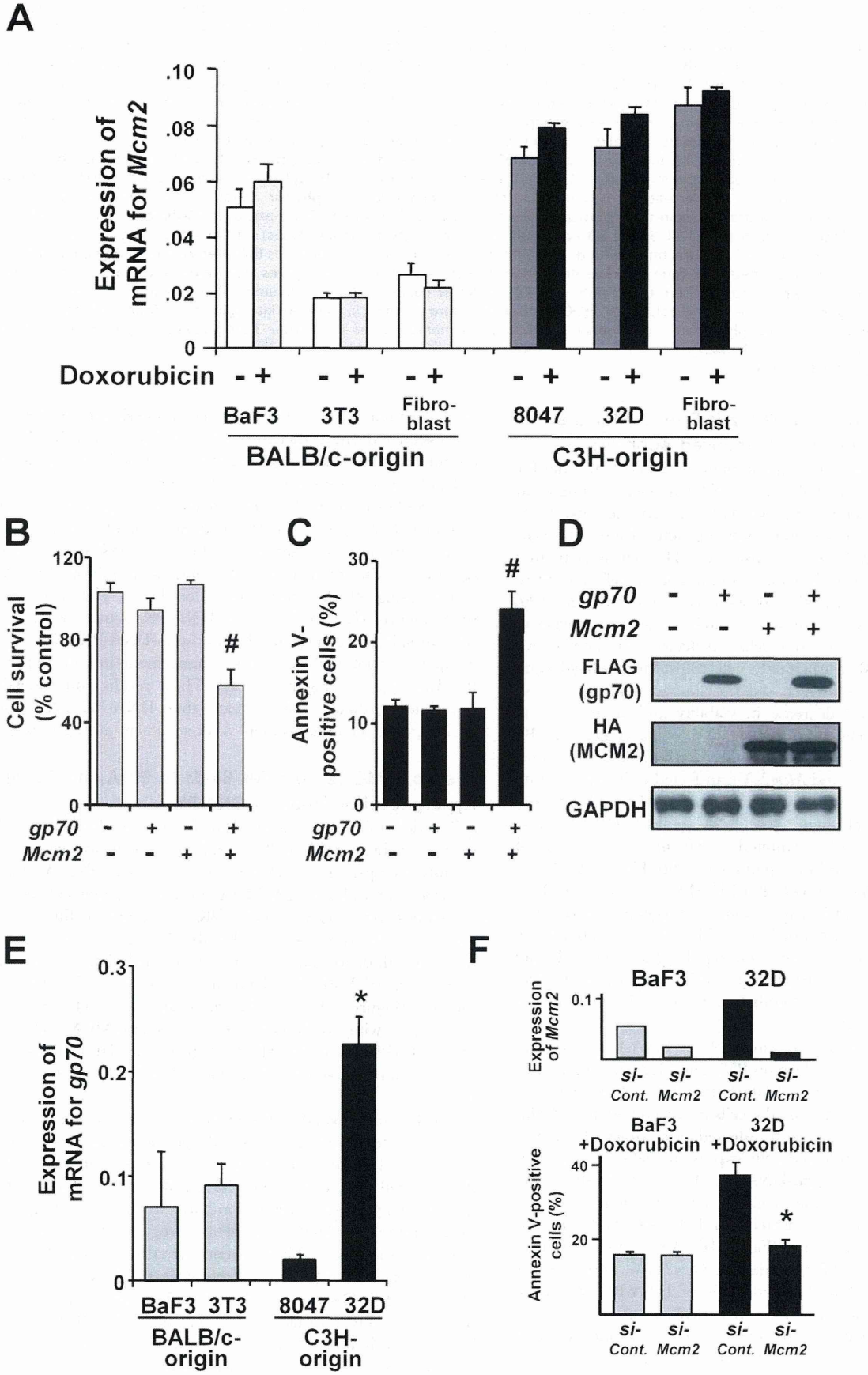
A
Expression of mRNA for Mcm2
.10
.08
.06
.04
.02
0
Doxorubicin - + - + - + - + - + - +
BaF3
3T3
Fibro-blast
8047
32D
Fibro-blast
BALB/c-origin
C3H-origin
B
Cell survival (% control)
120
80
40
0
#
gp70 - + - +
Mcm2 - - + +
C
Annexin V-positive cells (%)
30
20
10
0
#
gp70 - + - +
Mcm2 - - + +
D
gp70 - + - +
Mcm2 - - + +
FLAG (gp70)
HA (MCM2)
GAPDH
E
Expression of mRNA for gp70
0.3
0.2
0.1
0
*
BaF3 3T3
8047 32D
BALB/c-origin
C3H-origin
F
Expression of Mcm2
BaF3
32D
0.1
si-Cont. si-Mcm2 si-Cont. si-Mcm2
BaF3 +Doxorubicin
32D +Doxorubicin
Annexin V-positive cells (%)
40
20
*
si-Cont. si-Mcm2 si-Cont. si-Mcm2

Figure 2. Dual transfection of *gp70* and *Mcm2* enhances DNA-damage-induced apoptosis in 3T3 cells. (**A**) Quantitative RT-PCR analysis of *Mcm2* mRNA expression in untreated and doxorubicin-treated BALB/c-derived BaF3 and 3T3 cells, and primary cultured fibroblasts, and C3H-derived 8047 and 32D cells, and primary cultured fibroblasts. Data represent the mean and 95% CI of 3 independent experiments. (**B**) Cell survival (% of control) measured with the MTT assay in *gp70* and/or *Mcm2*-transfected 3T3 cells after treatment with doxorubicin for 24 h. Cell survival is significantly different between control cells "*gp70* (−), *Mcm2* (−)" and *gp70/Mcm2*-transfected cells "*gp70* (+), *Mcm2* (+)" (#$p<0.01$). Data represent the mean and 95% CI of 3 independent experiments. (**C**) Apoptotic cell ratios in *gp70* and/or *Mcm2*-transfected 3T3 cells were determined with annexin V-staining after treatment with 1 μM doxorubicin for 24 h. The ratios in the control cells "*gp70* (−), *Mcm2* (−)" and *gp70/Mcm2*-transfected cells "*gp70* (+), *Mcm2* (+)" are significantly different (#$p<0.01$). Data represent the mean and 95% CI of 3 independent experiments. (**D**) Western blot analysis of *gp70* and/or *Mcm2-FL*-transfected 3T3 cells after treatment with 1 μM of doxorubicin for 24 h. Gp70 and MCM2 protein levels are similar in all groups. (**E**) Expression of endogenous *gp70* mRNA in BaF3, 3T3, 8047, and 32D cells. G*p70* mRNA expression (ng) was normalized to that of *GAPDH*. Note the significantly higher expression of *gp70* mRNA in 32D cells compared to that in the other cells (*$p<0.01$). Data show the mean and 95% CI of three independent experiments. (**F**) *Mcm2* knockdown in BaF3 and 32D cells using siRNA. Quantitative RT-PCR (upper) was performed to confirm *si-Mcm2*-induced reduction of *Mcm2* mRNA expression. Apoptotic cell ratios were determined with annexin V-staining after treatment with doxorubicin for 24 h (bottom). Note the significant decrease in the apoptotic cell ratio of 32D cells treated with *si-Mcm2*, compared to that of cells treated with *si-Control* (*$p<0.01$). Data show the mean and 95% CI of 3 independent experiments.
doi:10.1371/journal.pone.0040129.g002

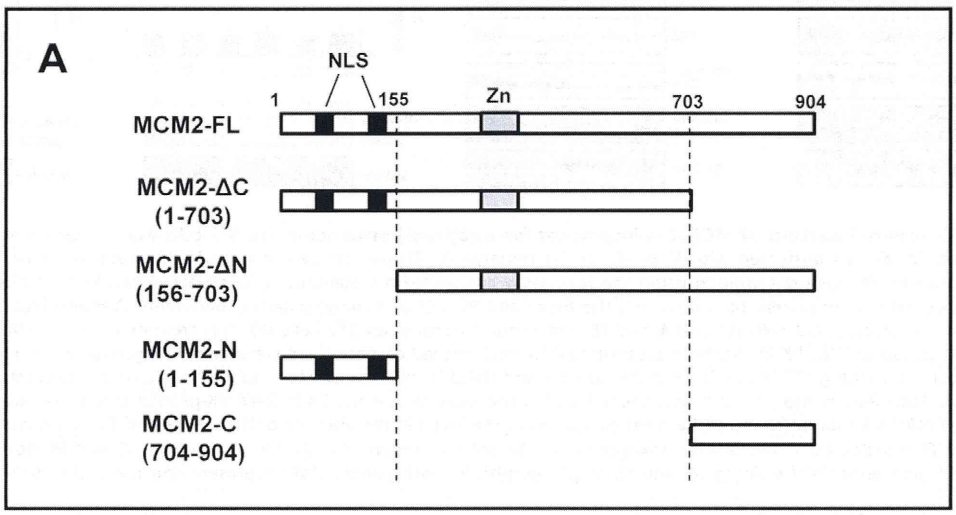

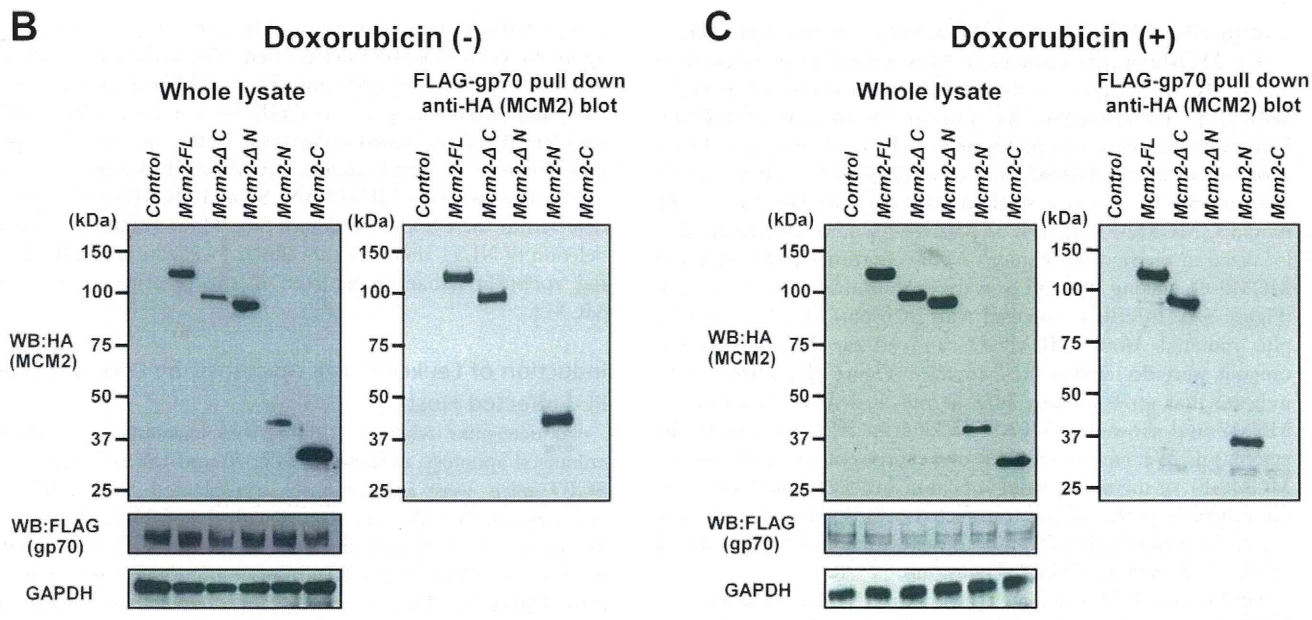

Figure 3. Direct interaction of MCM2 with gp70. (**A**) Schematic diagram of full-length MCM2 (MCM2-FL) and MCM2 deletion mutants, MCM2-ΔC (aa 1–703), MCM2-ΔN (aa 156–703), MCM2-N (aa 1–155) and MCM2-C (aa 704–904). The NLS domains are shown in black, and the Zn-finger domains are gray. 3T3 cells were transfected with *HA*-tagged *Mcm2* mutants along with *FLAG*-tagged *gp70*, and either left untreated (**B**) or treated with 1 μM doxorubicin for 24 h (**C**). The expression of the MCM2 mutants (**B**, **C**, left upper) and FLAG-gp70 (**B**, **C**, left middle) was confirmed in 3T3 cells. Cell lysates were subjected to a pull-down assay to detect the binding of MCM2-FL or MCM2 mutants to FLAG-gp70 (**B**, **C**, right panel).
doi:10.1371/journal.pone.0040129.g003

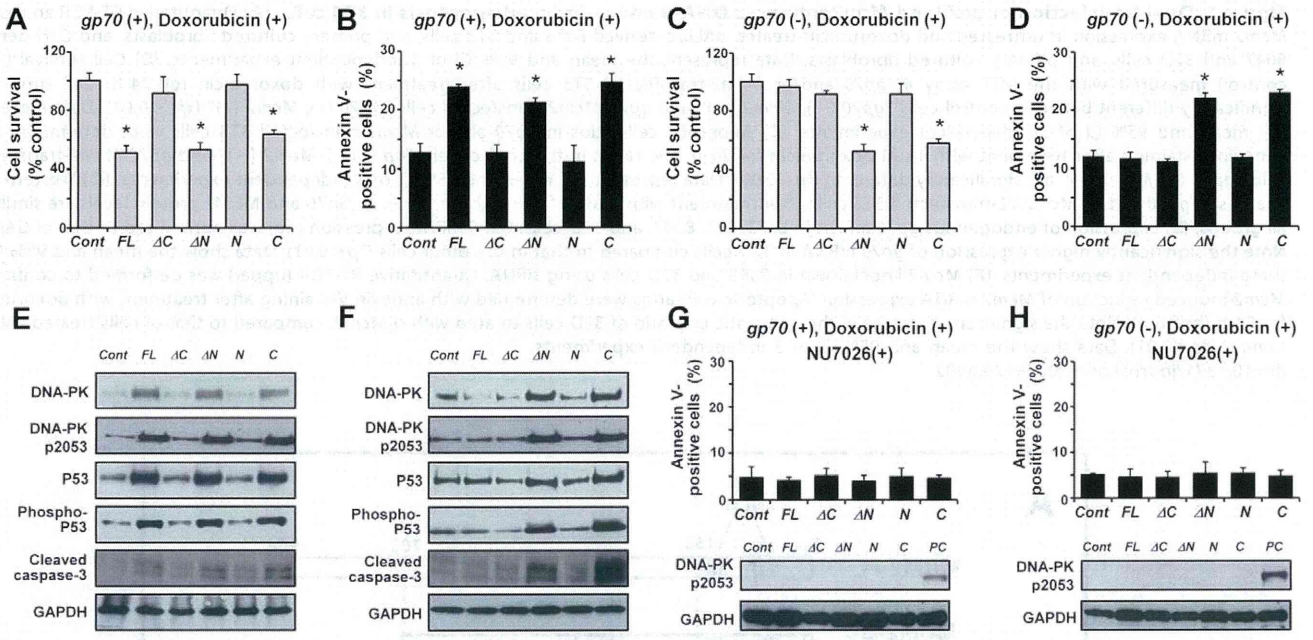

Figure 4. The C-terminal portion of MCM2 is important for apoptosis enhancement. 3T3 cells were co-taransfected with *gp70* and *Mcm2-FL* or the mutants (**A**, **B**) or transfected with *Mcm2-FL* or the mutants (**C**, **D**) and treated with 1 μM doxorubicin for 24 h. Cell survival (**A**, **C**) and apoptotic cell ratios (**B**, **D**) were determined using the MTT assay and annexin V-staining, respectively. Asterisks (*) indicate $p<0.01$ for control vs. mutant-transfected cells. In all panels, data represent the mean and 95% CI of 3 independent experiments. Western blot analysis of *gp70/Mcm2-FL*- and *gp70*/mutant-transfected 3T3 cells (**E**) and *Mcm2-FL*- and mutant-transfected 3T3 cells (**F**) after treatment with 1 μM doxorubicin for 24 h. The levels of DNA-PK, phospho-DNA-PK (pS2053), P53, phospho-P53, and cleaved caspase-3 are elevated in the groups with elevated apoptotic ratios. (**G**) 3T3 cells co-transfected with *gp70/Mcm2-FL* or *gp70*/mutants and (**H**) 3T3 cells transfected with *Mcm2-FL* or the mutants were pre-incubated with 10 μM NU7026, a DNA-PK-inhibitor, for 2 h and treated with 1 μM doxorubicin for 24 h. DNA-PK-pS2053 levels are substantially reduced in cells treated with the DNA-PK-inhibitor (**G** and **H**, bottom) compared to the levels in the absence of NU7026 (**E** and **F**, respectively). Whole cell lysates from *gp70*- and *Mcm2-FL*-transfected 3T3 cells after doxorubicin treatment are shown as a positive control (PC, **G** and **H**, bottom). Apoptotic cell ratios were determined with annexin V-staining (**G** and **H,** upper graph). In both panels, data represent the mean and 95% CI of three independent experiments.

doi:10.1371/journal.pone.0040129.g004

The gp70-MCM2 Complex is Localized in the Cytoplasm

The MCM2 protein contains an NLS in the N-terminal portion. Thus, MCM2 localizes to the nucleus when expressed in HeLa cells [47]. To investigate the cellular localization of MCM2, immunofluorescence was performed on 3T3 cells transfected with *Mcm2-FL* or mutated *Mcm2*, with or without *gp70* and treated with doxorubicin. In 3T3 cells singly transfected with *Mcm2-FL* or the mutants, MCM2-FL as well as MCM2-ΔC and MCM2-N were localized in the nucleus (Figure 6A). By contrast, MCM2-ΔN and MCM2-C lacking the NLS were localized in the cytoplasm (Figure 6A). In cells transfected with *gp70* plus *Mcm2-FL* or *gp70* plus mutated *Mcm2*, MCM2-FL and all the MCM2 deletion mutants were detected in the cytoplasm (Figure 6B). These results indicate that gp70 binding inhibits the nuclear translocation of MCM2 and show that MCM2 lacking an NLS remains in the cytoplasm. We confirmed that overexpression of gp70 and/or MCM2-FL or the mutants did not cause any significant changes in the cell-cycle profile of the transfected cells (Figure S5). Furthermore, the transfected gp70 induced the cytoplasmic localization of DNA-PK as well as MCM2 (Figure S6).

MCM2 has 2 NLS domains, NLS1 and NLS2. NLS2 but not NLS1 is required for the nuclear localization of mouse MCM2 [47]. Thus, to further examine the gp70-mediated inhibition of MCM2 nuclear translocation, we generated plasmids encoding HA-tagged MCM2 NLS deletions; deletion of NLS1 (MCM2-ΔNLS1), deletion of NLS2 (MCM2-ΔNLS1), and deletion of NLS1 to NLS2 (MCM2-ΔNLS1-2) (Figure 6C). 3T3 cells were transfected with these mutants and treated with doxorubicin, and apoptotic cell ratios were determined. The ratio was significantly increased in *Mcm2-ΔNLS2*- and *Mcm2-ΔNLS1-2*-transfected cells compared to the negative control. By contrast, *Mcm2-ΔNLS1*-transfected cells exhibited no increase in the number of apoptotic cells (Figure 6D). Furthermore, MCM2-ΔNLS1 was localized in the nucleus, whereas MCM2-ΔNLS2 and MCM2-ΔNLS1-2 were detected in the cytoplasm (Figure S7). These results indicate that deletion of NLS2 alters the subcellular localization of MCM2 and the apoptosis enhancement seen in the presence of the gp70-MCM2.

Induction of Leukemia cell Apoptosis by DNA-damage in FLV-infected Hosts

To determine whether C3H-derived leukemia cells exhibited enhanced apoptosis in response to gp70 and DNA-damage *in vivo*, SCID mice were intravenously transplanted with 8047 cells, inoculated with FLV, and treated with doxorubicin. As expected, the 8047 cell-containing liver samples from FLV-infected mice exhibited a stronger expression of *gp70* than those from uninfected mice (Figure 7A). Treatment with a low dose of doxorubicin caused significant enhancement of apoptosis in FLV-infected SCID mice but not in uninfected mice (Figure 7B, C). These results indicate that *gp70* overexpression and DNA-damage induction elicit significant apoptosis of C3H-derived leukemia cells *in vivo*.

Next, to investigate the subcellular localization of MCM2 in the transplanted 8047 cells from hepatic nodules, immunohistochem-

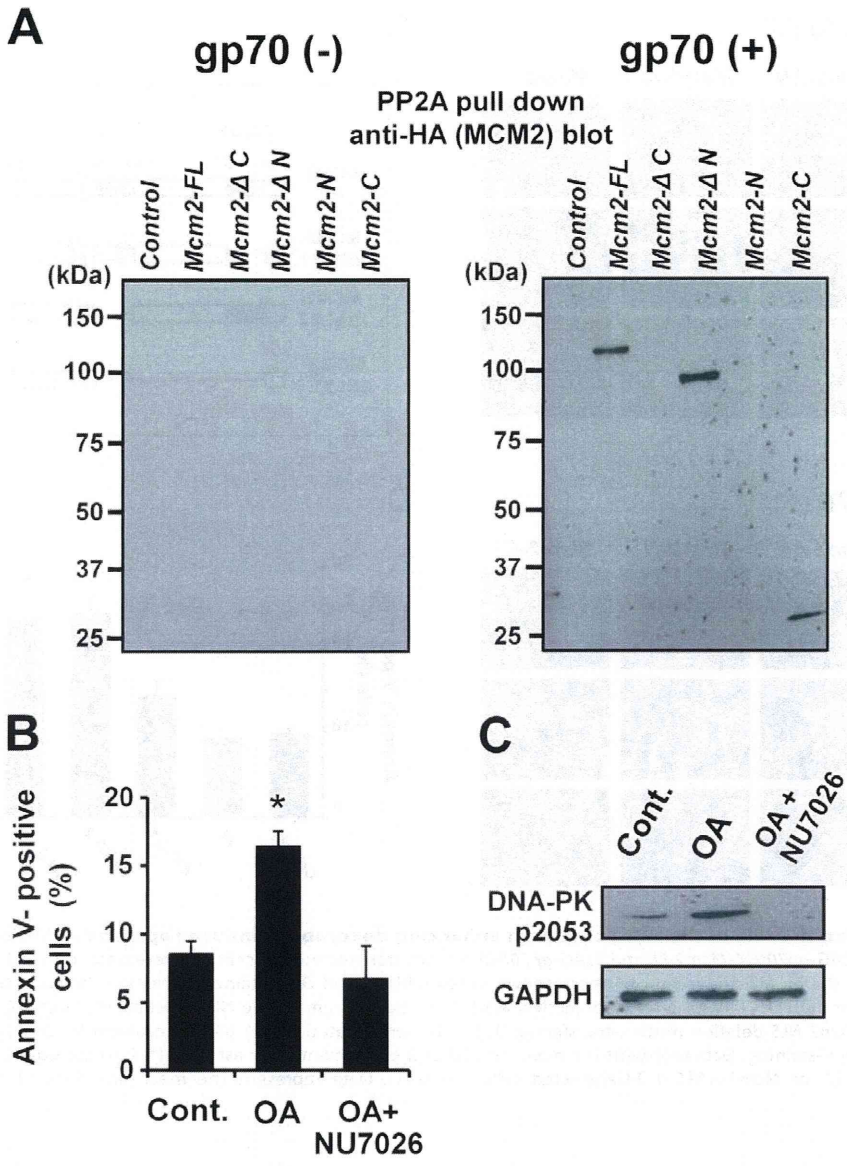

Figure 5. MCM2 (FL and mutants) interacts with PP2A. (**A**) The *Mcm2-FL*- or mutant-transfected 3T3 cells (left) and *gp70/Mcm2-FL*- or *gp70/* mutants-transfected 3T3 cells (right) were treated with 1 μM doxorubicin for 24 h. Cell lysates were subjected to a pull-down assay to detect the binding of MCM2-FL or the mutants to PP2A. (**B**) 3T3 cells were pre-incubated with 10 nM okadaic acid (OA) and 10 μM NU7026 for 2 h, and treated with 1 μM doxorubicin for 24 h. The apoptotic cell ratio was determined with annexin V-staining. Asterisk (*) indicates $p<0.01$ for control vs. mutant-transfected cells. Data represent the mean and 95% CI of 3 independent experiments. (**C**) Western blot analysis of 3T3 cells to detect phospho-DNA-PK. Note the significantly increased levels of DNA-PK-p2053 in OA-treated 3T3 cells, and the complete abrogation by NU7026.
doi:10.1371/journal.pone.0040129.g005

istry was performed. MCM2 was localized in the nucleus of 8047 cells in uninfected SCID mice (Figure 7D, top), whereas some 8047 cells exhibited cytoplasmic MCM2 in the FLV-infected mice (Figure 7D, bottom). Furthermore, the number of cells with cytoplasmic MCM2 was remarkably increased in FLV-infected doxorubicin-treated mice compared to FLV-infected PBS-treated mice (Figure 7D, bottom right and E).

A survival analysis was performed on mice treated with PBS or doxorubicin twice a week. FLV-infected and doxorubicin-treated mice exhibited a significant improvement in survival compared to the other groups (Figure 7F). These results suggest significant effects of cytoplasmic MCM2 on apoptosis induction in leukemia cells in the *in vivo* model. Although not so remarkable, FLV-infection alone prolonged the survival of 8047 cell-transplanted mice. The phenomenon may be caused by intrinsic host defense mechanisms such as innate immunity systems and inflammatory reactions by natural killer cells, neutrophils, monocyte/macrophages etc., against leukemia cells. The reactions may include reactive oxygen species or other stress signaling pathways associated with DNA-damage induction. Thus, the circulating leukemia cells may differ from the leukemia cells used *in vitro* experiments without any stimulation for DNA-damage.

Discussion

A novel strategy for controlling tumor cell growth is to target regulators of cellular proliferation/apoptosis. However, the cellular dynamics of non-tumor cells should not be influenced by

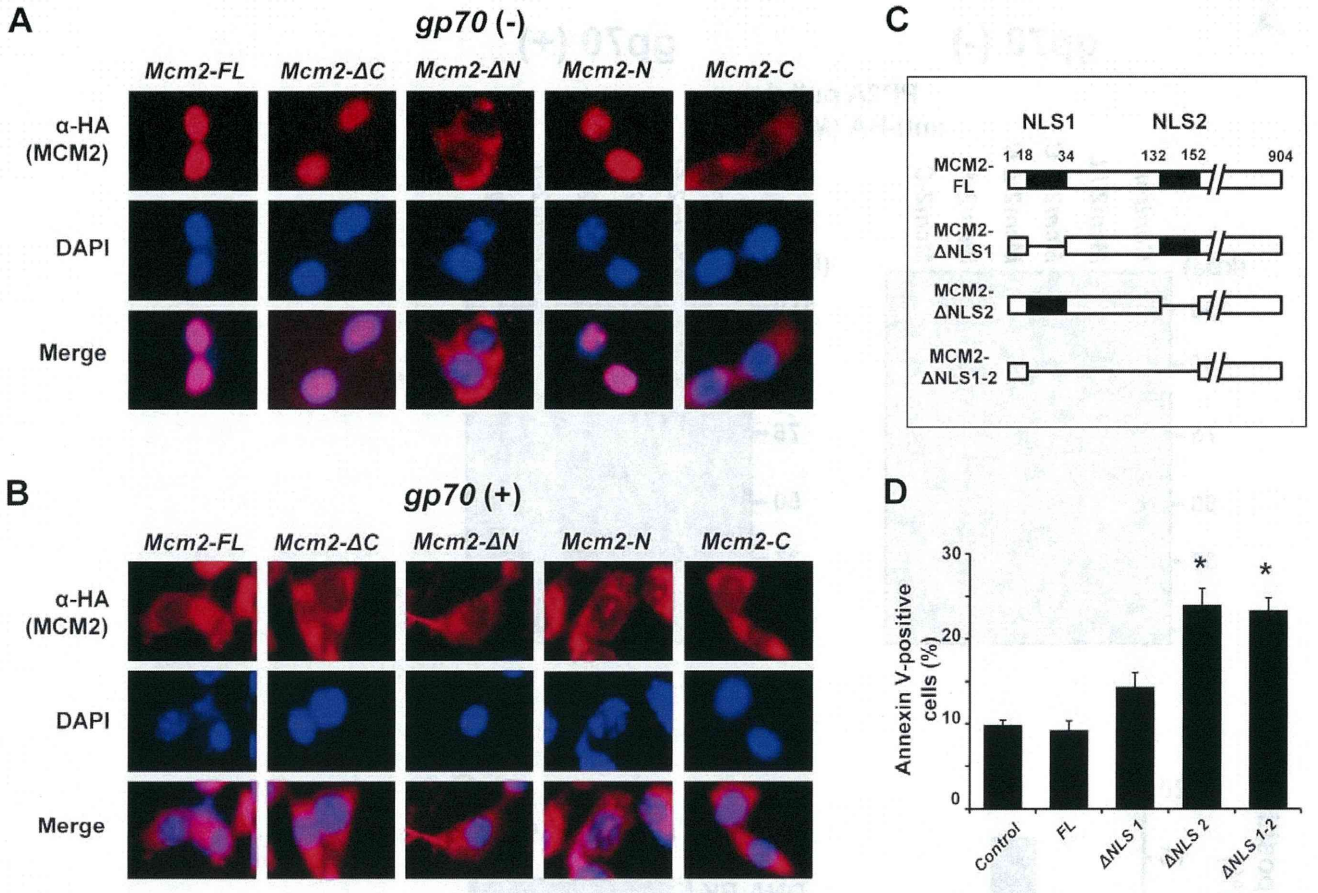

Figure 6. Subcellular localization of MCM2 and the role of the NLS domains in enhancing doxorubicin-induced apoptosis. *HA-Mcm2-FL* and *HA*-mutant-transfected 3T3 cells (**A**), and *FLAG-gp70/HA-Mcm2-FL* and *FLAG-gp70/HA*-mutant-transfected 3T3 cells (**B**) were treated with 1 μM doxorubicin for 24 h. HA-positive cells containing the MCM2-derived proteins are shown in red (TRITC), and DAPI-stained nuclei are shown in blue. Images were acquired using a BZ-9000 microscope (KEYENCE) with a 400× objective. (**C**) Schematic diagram of the NLS deletion mutants MCM2-ΔNLS1, MCM2-ΔNLS2, and MCM2-ΔNLS1-2. (**D**) *Mcm2-NLS* deletion mutant-transfected 3T3 cells were treated with 1 μM doxorubicin for 24 h, and apoptotic cell ratios were determined with annexin V-staining. Data represent the mean and SD of 3 experiments. The asterisks (*) indicate significant differences between the control and *Mcm2-ΔNLS2-* or *Mcm2-ΔNLS 1-2*-transfected cells (*$p<0.01$). Data represent the mean and 95% CI of 3 independent experiments.
doi:10.1371/journal.pone.0040129.g006

these treatments. This is very difficult, but infection with certain types of viruses elicits tumor cell-specific changes in cellular dynamics [48]. Thus, virus-host interaction may provide clues to develop a novel strategy for tumor therapy. Our previous study has shown that FLV infection strongly enhances radiation-induced apoptosis in the hematopoietic cells of C3H mice, although the response is not uniform among the host strains [17]. Elucidation of the molecular mechanisms underlying this host- and cell type-specificity may provide an effective means to induce tumor cell-specific apoptosis in host tissues.

Regarding host specificity, MCM2 was identified as a C3H-specific protein that enhances DNA-damage-induced apoptosis in association with the envelope protein of FLV, gp70. However, MCM2 is part of a conserved set of MCM proteins (MCM2-7), with essential roles in the regulation of DNA replication: functioning as license components for S-phase initiation and further acting as a helicase to unwind DNA at replication forks [25,26,49]. Indeed, MCM proteins are frequently overexpressed in a variety of cancer or pre-cancerous cells [31–36]. In this study, *Mcm2*-transfected 3T3 cells exhibited an increase in proliferation 96 h after transfection. On the other hand, co-transfection of BALB/c-derived 3T3 cells, which originally expressed low levels of *Mcm2*, with *gp70* and *Mcm2* enhanced doxorubicin-induced apoptosis. These results suggest that human tumor cells may also become more sensitive to DNA-damage-induced apoptosis through changes in the molecular functions of MCM2.

MCM2 has several functional domains [50]. However, there are no reports on its functions in apoptosis. Our study demonstrated that a novel functional domain in the C-terminal portion of MCM2 plays a role in apoptosis enhancement under specific conditions in conjunction with gp70 (Figure 8A).

MCM2 is known to interact with various types of molecules, including protein PP2A [51]. PP2A is one of the major Ser/Thr phosphatases implicated in the regulation of cellular processes such as cell cycle progression [52], apoptotic cell death [53–55], and DNA replication and DSB repair [45,52,53]. In the GeneChip assay of the present study, *Ppp2ac* exhibited an expression pattern similar to that of *Mcm2* in the *in vivo* experiments (correlation coefficient >90%; Figure 1L, Table S1). Furthermore, our results suggest that PP2A dephosphorylates DNA-PK and regulates its function, as described previously [44–46]. Depletion of PP2A by RNAi has been shown to induce hyperphosphorylation of DNA-PK and suppression of DNA end-joining followed by enhanced cytogenetic abnormalities including chromosomal and chromatid

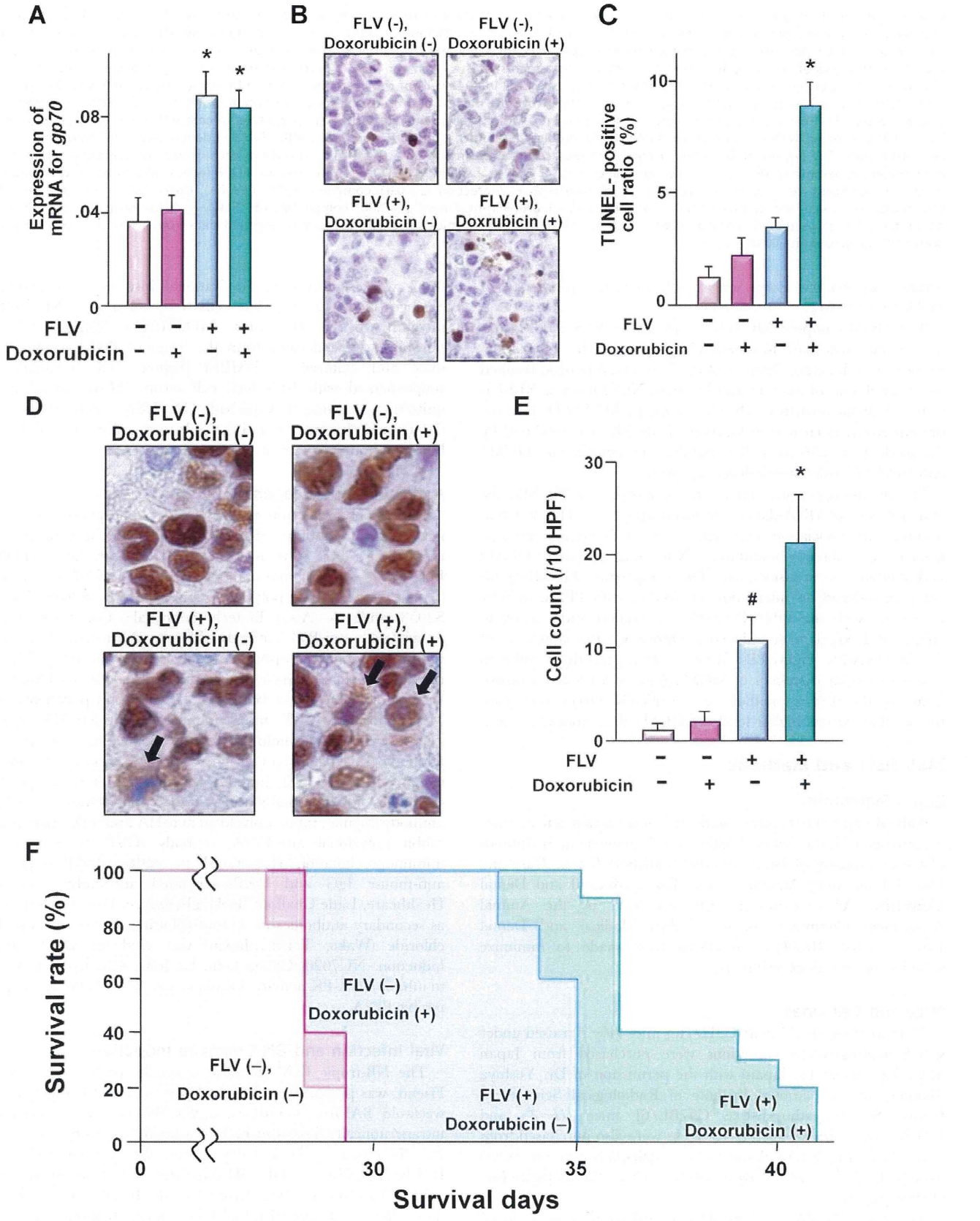

Figure 7. ***In vivo*** **anti-tumor effects of** ***gp70*** **expression and DNA-damage on the C3H-derived cells in SCID mice.** Two weeks after transplantation, mice were inoculated (i.p.) with FLV. Seven days later, the mice were treated with 1.5 mg/kg of doxorubicin or PBS. (**A**) Quantitative RT-PCR analysis of *gp70* mRNA expression in the liver of SCID mice with multiple foci of leukemic infiltration. The samples from FLV-infected mice

exhibit higher levels of *gp70* than those from uninfected mice (*$p<0.01$). Data represent the mean and 95% CI of from 10 mice in each group and are representative of 2 independent experiments. (**B**) Microscopic features of TUNEL-positive cells in hepatic nodules and (**C**) TUNEL-positive cell ratio in each group of mice. Note the significant increase in apoptotic 8047 cells in mice with FLV infection and doxorubicin treatment (*$p<0.01$ compared with the tumor cells of "FLV (−), doxorubicin (−) mice"). Data represent the mean and 95% CI of from 10 mice in each group and are representative of 2 independent experiments. (**D**) Subcellular localization of MCM2 in 8047 cells of the liver demonstrated by immunohistochemistry. Images were captured with a microscope at 1,000× magnification power. Note the nuclear and/or cytoplasmic localization of MCM2 in the 8047 cells from each group of mice. (**E**) The cell counts for cytoplasmic localization of MCM2. Cell counts are shown as the number of cells per 10 high-power fields (HPF). [# $p<0.01$ compared with tumor cells of "FLV (−), doxorubicin (−)" mice; *$p<0.001$ compared with "FLV (−) doxorubicin (−)" mice and $p<0.05$ compared with "FLV (+), doxorubicin (−)" mice]. Data represent the mean and 95% CI of from 10 mice in each group and are representative of 2 independent experiments. (**F**) Kaplan-Meier survival curves for 8047-transplanted SCID mice with/without FLV-infection and doxorubicin-treatment. Note the significant elongation of survival time in mice with FLV-infection [$p<0.01$ compared with "FLV (−), doxorubicin (−)" and "FLV (−), doxorubicin (+)" mice] and in mice with FLV-infection and doxorubicin-treatment [$p<0.001$ compared with "FLV (−), doxorubicin (−)" and "FLV (−), doxorubicin (+)" mice, $p<0.01$ compared with "FLV (+), doxorubicin (−)" mice]. The survival curves represent data from 10 mice in each group.
doi:10.1371/journal.pone.0040129.g007

breaks [46]. Similar events may result from the interaction of PP2A with MCM2.

The MCM complex (MCM2-7) contains an NLS. MCM2 has 2 NLS domains and histone-binding sites in the N-terminal portion, and therefore deletion of the N-terminal portion resulted in the inhibition of nuclear translocation. NLS2 but not NLS1 is required for the nuclear localization of mouse MCM2 [47]. In the present study, nuclear translocation of MCM2 was inhibited by the binding of gp70 to NLS1, and that the cytoplasmic MCM2 enhanced DNA-damage-induced apoptosis.

In conclusion, we identified a novel function of MCM2: the enhancement of DNA-damage-induced apoptosis. This function occurred in association with gp70, an FLV-derived envelope protein. Gp70 directly bound to the N-terminal portion of MCM2 and inhibited its translocation. The cytoplasmic MCM2-gp70-complex induced an interaction of MCM2 with PP2A, thereby interfering with the PP2A-DNA-PK interaction and leading to enhanced DNA-damage-induced apoptosis via the activation of P53 by DNA-PK (Figure 8B). These results suggest that regulation of the molecular dynamics of MCM2 may be a novel apoptosis-inducing therapeutic method to specifically target malignant tumors that express higher levels of MCM2 than normal tissues.

Materials and Methods

Ethics Statement

Animal experiments were conducted and carried out in strict accordance with the Act on Welfare and Management of Animals of the government of Japan and the Guidelines for the Care and Use of Laboratory Animals of the Tokyo Medical and Dental University. All experiments were approved by the Animal Experiment Committee of the Tokyo Medical and Dental University (No. 100115). All efforts were made to minimize suffering in animal experiments.

Mice and Cell Lines

Eight to 10-week-old male C3H/HeJ mice ($H-2^b$) raised under specific-pathogen-free conditions were purchased from Japan SLC, Inc. (Shizuoka, Japan) with the permission of Dr. Yoshiya Shimada of the National Institute of Radiological Sciences in Chiba. Specific-pathogen-free C57BL/6J mice ($H-2^b$) and BALB/c mice ($H-2^d$) aged 8–10 weeks were also purchased from Japan SLC, Inc. Six-week-old male specific-pathogen-free SCID mice (C.B.17$^{scid/scid}$, $H-2^d$) were purchased from CLEA Japan Inc. (Tokyo, Japan).

The mouse fibroblast cell line 3T3 and the mouse acute myeloid leukemia cell line, BaF3, both derived from BALB/c mice, and the C3H mouse bone marrow cell-derived 32D cells were purchased from the RIKEN Cell Bank (Tsukuba, Ibaraki, Japan). The radiation-induced myeloid leukemia cell line from C3H mice, 8047, was established at the National Institute of Radiological Sciences in Chiba [22]. The cells were cultured in RPMI-1640 medium (Sigma, St. Louis, MO, USA). Primary cultured fibroblasts were derived from the lungs of BALB/c and C3H mice and cultured in DMEM (Sigma). The medium was supplemented with 10% fetal calf serum (FCS), penicillin (50 units/mL) (Invitrogen, Carlsbad, CA, USA), and streptomycin (50 μg/mL) (Invitrogen) and the cells were cultured at 37°C in a humidified atmosphere of 5% CO_2 in air.

Antibodies and Reagents

Rabbit polyclonal anti-glyceraldehyde-3-phosphate dehydrogenase (GAPDH) antibody (Santa Cruz Biotechnology, Santa Cruz, CA, USA), rabbit polyclonal anti-ATM antibody (MILLIPORE, Billerica, MA, USA), mouse monoclonal anti-DNA-PK$_{cs}$ antibody (Santa Cruz), rabbit polyclonal anti-DNA-PK S2056 (Mouse-S2053) antibody (Assay Biotech, Sunnyvale, CA, USA), mouse monoclonal anti-P53 antibody (Merck, Darmstadt, Germany), rabbit polyclonal anti-phospho-P53 (Ser 15) antibody (Merck), rabbit monoclonal anti-cleaved caspase-3 antibody (Cell Signaling Technology [CST], Danvers, MA, USA), rabbit polyclonal anti-MCM3 antibody (CST), mouse monoclonal anti-MCM4 antibody (Santa Cruz Biotechnology), mouse monoclonal anti-HA tag antibody (Invivogen, San Diego, CA, USA), and mouse monoclonal anti-FLAG M2 antibody (Sigma) were used as primary antibodies for immunoblotting. Rabbit polyclonal anti-FLAG antibody (Sigma), rabbit polyclonal anti-HA antibody (Sigma), and rabbit polyclonal anti-PP2A antibody (CST) were used for immunoprecipitation. Horseradish peroxidase (HRP)-conjugated anti-mouse IgG and HRP-conjugated anti-rabbit IgG (GE Healthcare, Little Chalfont Buckinghamshire, England) were used as secondary antibodies for immunoblotting. Doxorubicin hydrochloride (Wako, Tokyo, Japan) was used for DNA-damage induction. NU7026 (Calbiochem, La Jolla, CA, USA) was used to inhibit DNA-PK activity. Okadaic acid (OA; Wako) was used to inhibit PP2A.

Viral Infection and DNA-damage Induction

The NB-tropic FLV complex, originally provided by Dr. C. Friend, was prepared as described previously [56]. Eight- to 10-week-old BALB/c, C57BL/6, and C3H mice were inoculated intraperitoneally (i.p.) with FLV at a highly leukemogenic dose of 10^4 PFU/mouse [57]. On day 7 after the infection with FLV, BALB/c, C57BL/6, and C3H mice were administered (i.p.) with 1.5 mg/kg of doxorubicin hydrochloride. In experiments *in vitro*, 3T3 cells were treated with 1 μM doxorubicin to induce apoptosis.

Detection of Apoptotic Cells

To determine the apoptotic cell ratios in mouse bone marrow and spleen cells after treatment with 1.5 mg/kg of doxorubicin for

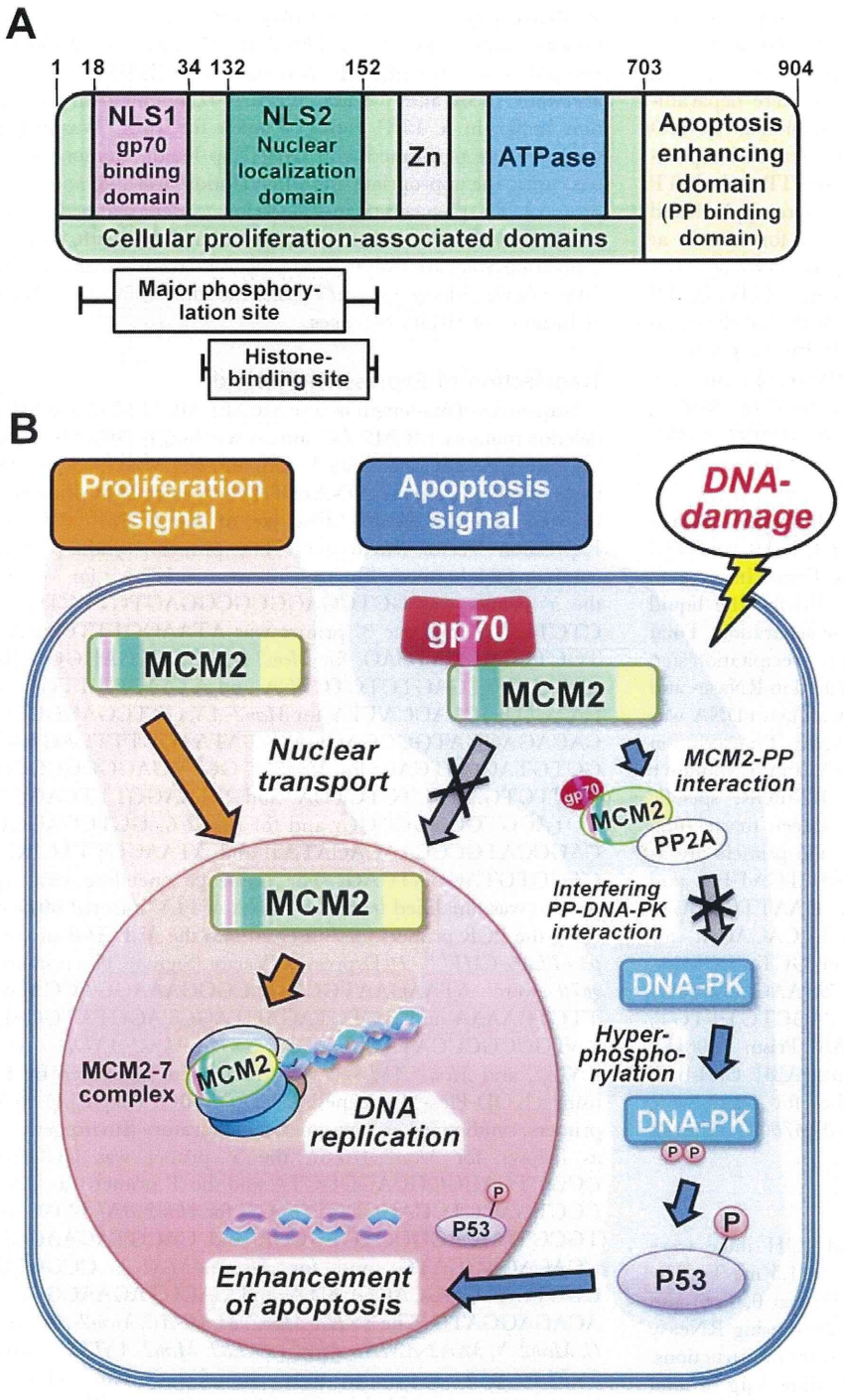

Figure 8. Schematic illustration of the structure of MCM2 and its functions in the cytoplasm and nucleus. (**A**) The various functional domains of the MCM2 protein are shown, and the domains and regions required for the activities are indicated. (**B**) Schematic of the novel role of MCM2 in apoptosis enhancement. Normally, MCM2 is recruited into the nucleus for participation in DNA replication. As a result, cellular proliferation is upregulated (proliferation signal). However, when gp70 is present in the cytoplasm, it binds to MCM2 and inhibits its nuclear entry. Furthermore, cytoplasmic gp70-MCM2-complex interacts with PP2A and inhibits its interaction with DNA-PK. Consequently, hyperphosphorylated DNA-PK enhances DNA-damage-induced apoptosis via a P53-related pathway (apoptosis signal).
doi:10.1371/journal.pone.0040129.g008

24 h, samples were collected from each experimental group, washed with ice-cold PBS, stained with propidium iodide (BD Biosciences, San Jose, CA, USA) and fluorescein isothiocyanate (FITC)-labeled anti-annexin V antibody (BD), and analyzed on a FACScan flow cytometer (BD FACSCanto^{TM} Flow Cytometer). To determine the apoptotic cell ratios in 32D, BaF3, and 3T3 cells after treatment with 1 μM doxorubicin for 24 h, samples were collected from each experimental group and washed with ice-cold PBS. These samples were stained with propidium iodide (PI), incubated with FITC-labeled anti-annexin V antibody, and